ARTICLES

Studies of topological distributions of inclusive three- and four-jet events in $\overline{pp}$ collisions at $\sqrt{s}=1800$ GeV with the D0 detector

S. Abachi,[12] B. Abbott,[34] M. Abolins,[23] B.S. Acharya,[42] I. Adam,[10] D. L. Adams,[35] M. Adams,[15] S. Ahn,[12] H. Aihara,[20] J. Alitti,[38] G. Álvarez,[16] G. A. Alves,[8] E. Amidi,[27] N. Amos,[22] E. W. Anderson,[17] S. H. Aronson,[3] R. Astur,[40] R. E. Avery,[29] A. Baden,[21] V. Balamurali,[30] J. Balderston,[14] B. Baldin,[12] J. Bantly,[4] J. F. Bartlett,[12] K. Bazizi,[37] J. Bendich,[20] S. B. Beri,[32] I. Bertram,[35] V. A. Bezzubov,[33] P. C. Bhat,[12] V. Bhatnagar,[32] M. Bhattacharjee,[11] A. Bischoff,[7] N. Biswas,[30] G. Blazey,[12] S. Blessing,[13] P. Bloom,[5] A. Boehnlein,[12] N. I. Bojko,[33] F. Borcherding,[12] J. Borders,[37] C. Boswell,[7] A. Brandt,[12] R. Brock,[23] A. Bross,[12] D. Buchholz,[29] V. S. Burtovoi,[33] J. M. Butler,[12] W. Carvalho,[8] D. Casey,[37] H. Castilla-Valdez,[9] D. Chakraborty,[40] S. -M. Chang,[27] S. V. Chekulaev,[33] L. -P. Chen,[20] W. Chen,[40] L. Chevalier,[38] S. Chopra,[32] B. C. Choudhary,[7] J. H. Christenson,[12] M. Chung,[15] D. Claes,[40] A. R. Clark,[20] W. G. Cobau,[21] J. Cochran,[7] W. E. Cooper,[12] C. Cretsinger,[37] D. Cullen-Vidal,[4] M. A. C. Cummings,[14] D. Cutts,[4] O. I. Dahl,[20] K. De,[43] M. Demarteau,[12] R. Demina,[27] K. Denisenko,[12] N. Denisenko,[12] D. Denisov,[12] S. P. Denisov,[33] W. Dharmaratna,[13] H. T. Diehl,[12] M. Diesburg,[12] G. Di Loreto,[23] R. Dixon,[12] P. Draper,[43] J. Drinkard,[6] Y. Ducros,[38] S. R. Dugad,[42] S. Durston-Johnson,[37] D. Edmunds,[23] J. Ellison,[7] V. D. Elvira,[12,*] R. Engelmann,[40] S. Eno,[21] G. Eppley,[35] P. Ermolov,[24] O. V. Eroshin,[33] V. N. Evdokimov,[33] S. Fahey,[23] T. Fahland,[4] M. Fatyga,[3] M. K. Fatyga,[37] J. Featherly,[3] S. Feher,[40] D. Fein,[2] T. Ferbel,[37] G. Finocchiaro,[40] H. E. Fisk,[12] Y. Fisyak,[5] E. Flattum,[23] G. E. Forden,[2] M. Fortner,[28] K. C. Frame,[23] P. Franzini,[10] S. Fuess,[12] E. Gallas,[43] A. N. Galyaev,[33] S. G. Gao,[12,†] T. L. Geld,[23] R. J. Genik II,[23] K. Genser,[12] C. E. Gerber,[12,‡] B. Gibbard,[3] V. Glebov,[37] S. Glenn,[5] B. Gobbi,[29] M. Goforth,[13] A. Goldschmidt,[20] B. Gómez,[1] P. I. Goncharov,[33] J. L. González Solís,[9] H. Gordon,[3] L. T. Goss,[44] N. Graf,[3] P. D. Grannis,[40] D. R. Green,[12] J. Green,[28] H. Greenlee,[12] G. Griffin,[6] N. Grossman,[12] P. Grudberg,[20] S. Grünendahl,[37] W. X. Gu,[12,†] G. Guglielmo,[31] J. A. Guida,[40] J. M. Guida,[3] W. Guryn,[3] S. N. Gurzhiev,[33] P. Gutierrez,[31] Y. E. Gutnikov,[33] N. J. Hadley,[21] H. Haggerty,[12] S. Hagopian,[13] V. Hagopian,[13] K. S. Hahn,[37] R. E. Hall,[6] S. Hansen,[12] R. Hatcher,[23] J. M. Hauptman,[17] D. Hedin,[28] A. P. Heinson,[7] U. Heintz,[12] R. Hernández-Montoya,[9] T. Heuring,[13] R. Hirosky,[13] J. D. Hobbs,[12] B. Hoeneisen,[1,§] J. S. Hoftun,[4] F. Hsieh,[22] Tao Hu,[12,†] Ting Hu,[40] Tong Hu,[16] T. Huehn,[7] S. Igarashi,[12] A. S. Ito,[12] E. James,[2] J. Jaques,[30] S. A. Jerger,[23] J. Z. -Y. Jiang,[40] T. Joffe-Minor,[29] H. Johari,[27] K. Johns,[2] M. Johnson,[12] H. Johnstad,[41] A. Jonckheere,[12] M. Jones,[14] H. Jöstlein,[12] S. Y. Jun,[29] C. K. Jung,[40] S. Kahn,[3] G. Kalbfleisch,[31] J. S. Kang,[18] R. Kehoe,[30] M. L. Kelly,[30] A. Kernan,[7] L. Kerth,[20] C. L. Kim,[18] S. K. Kim,[39] A. Klatchko,[13] B. Klima,[12] B. I. Klochkov,[33] C. Klopfenstein,[5] V. I. Klyukhin,[33] V. I. Kochetkov,[33] J. M. Kohli,[32] D. Koltick,[34] A. V. Kostritskiy,[33] J. Kotcher,[3] J. Kourlas,[26] A. V. Kozelov,[33] E. A. Kozlovski,[33] M. R. Krishnaswamy,[42] S. Krzywdzinski,[12] S. Kunori,[21] S. Lami,[40] G. Landsberg,[12] J. -F. Lebrat,[38] A. Leflat,[24] H. Li,[40] J. Li,[43] Y. K. Li,[29] Q. Z. Li-Demarteau,[12] J. G. R. Lima,[36] D. Lincoln,[22] S. L. Linn,[13] J. Linnemann,[23] R. Lipton,[12] Y. C. Liu,[29] F. Lobkowicz,[37] S. C. Loken,[20] S. Lökös,[40] L. Lueking,[12] A. L. Lyon,[21] A. K. A. Maciel,[8] R. J. Madaras,[20] R. Madden,[13] I. V. Mandrichenko,[33] Ph. Mangeot,[38] S. Mani,[5] B. Mansoulié,[38] H. S. Mao,[12,†] S. Margulies,[15] R. Markeloff,[28] L. Markosky,[2] T. Marshall,[16] M. I. Martin,[12] M. Marx,[40] B. May,[29] A. A. Mayorov,[33] R. McCarthy,[40] T. McKibben,[15] J. McKinley,[23] T. McMahon,[31] H. L. Melanson,[12] J. R. T. de Mello Neto,[36] K. W. Merritt,[12] H. Miettinen,[35] A. Milder,[2] A. Mincer,[26] J. M. de Miranda,[8] C. S. Mishra,[12] M. Mohammadi-Baarmand,[40] N. Mokhov,[12] N. K. Mondal,[42] H. E. Montgomery,[12] P. Mooney,[1] M. Mudan,[26] C. Murphy,[16] C. T. Murphy,[12] F. Nang,[4] M. Narain,[12] V. S. Narasimham,[42] A. Narayanan,[2] H. A. Neal,[22] J. P. Negret,[1] E. Neis,[22] P. Nemethy,[26] D. Nešić,[4] M. Nicola,[8] D. Norman,[44] L. Oesch,[22] V. Oguri,[36] E. Oltman,[20] N. Oshima,[12] D. Owen,[23] P. Padley,[35] M. Pang,[17] A. Para,[12] C. H. Park,[12] Y. M. Park,[19] R. Partridge,[4] N. Parua,[42] M. Paterno,[37] J. Perkins,[43] A. Peryshkin,[12] M. Peters,[14] H. Piekarz,[13] Y. Pischalnikov,[34] A. Pluquet,[38]

V. M. Podstavkov,[33] B. G. Pope,[23] H. B. Prosper,[13] S. Protopopescu,[3] D. Pušeljić,[20] J. Qian,[22] P. Z. Quintas,[12] R. Raja,[12] S. Rajagopalan,[40] O. Ramirez,[15] M. V. S. Rao,[42] P. A. Rapidis,[12] L. Rasmussen,[40] A. L. Read,[12] S. Reucroft,[27] M. Rijssenbeek,[40] T. Rockwell,[23] N. A. Roe,[20] P. Rubinov,[40] R. Ruchti,[30] S. Rusin,[24] J. Rutherfoord,[2] A. Santoro,[8] L. Sawyer,[43] R. D. Schamberger,[40] H. Schellman,[29] J. Sculli,[26] E. Shabalina,[24] C. Shaffer,[13] H. C. Shankar,[42] Y. Y. Shao,[12,†] R. K. Shivpuri,[11] M. Shupe,[2] J. B. Singh,[32] V. Sirotenko,[28] W. Smart,[12] A. Smith,[2] R. P. Smith,[12] R. Snihur,[29] G. R. Snow,[25] S. Snyder,[40] J. Solomon,[15] P. M. Sood,[32] M. Sosebee,[43] M. Souza,[8] A. L. Spadafora,[20] R. W. Stephens,[43] M. L. Stevenson,[20] D. Stewart,[22] D. A. Stoianova,[33] D. Stoker,[6] K. Streets,[26] M. Strovink,[20] A. Sznajder,[8] A. Taketani,[12] P. Tamburello,[21] J. Tarazi,[6] M. Tartaglia,[12] T. L. Taylor,[29] J. Teiger,[38] J. Thompson,[21] T. G. Trippe,[20] P. M. Tuts,[10] N. Varelas,[23] E. W. Varnes,[20] P. R. G. Virador,[20] D. Vititoe,[2] A. A. Volkov,[33] A. P. Vorobiev,[33] H. D. Wahl,[13] G. Wang,[13] J. Wang,[12,†] J. Warchol,[30] M. Wayne,[30] H. Weerts,[23] F. Wen,[13] W. A. Wenzel,[20] A. White,[43] J. T. White,[44] J. A. Wightman,[17] J. Wilcox,[27] S. Willis,[28] S. J. Wimpenny,[7] J. V. D. Wirjawan,[44] J. Womersley,[12] E. Won,[37] D. R. Wood,[12] H. Xu,[4] R. Yamada,[12] P. Yamin,[3] C. Yanagisawa,[40] J. Yang,[26] T. Yasuda,[27] C. Yoshikawa,[14] S. Youssef,[13] J. Yu,[37] Y. Yu,[39] D. H. Zhang,[12,†] Y. Zhang,[12,†] Q. Zhu,[26] Z. H. Zhu,[37] D. Zieminska,[16] A. Zieminski,[16] and A. Zylberstejn[38]

(D0 Collaboration)

[1]*Universidad de los Andes, Bogotá, Colombia*
[2]*University of Arizona, Tucson, Arizona 85721*
[3]*Brookhaven National Laboratory, Upton, New York 11973*
[4]*Brown University, Providence, Rhode Island 02912*
[5]*University of California, Davis, California 95616*
[6]*University of California, Irvine, California 92717*
[7]*University of California, Riverside, California 92521*
[8]*LAFEX, Centro Brasileiro de Pesquisas Físicas, Rio de Janeiro, Brazil*
[9]*CINVESTAV, Mexico City, Mexico*
[10]*Columbia University, New York, New York 10027*
[11]*Delhi University, Delhi, India 110007*
[12]*Fermi National Accelerator Laboratory, Batavia, Illinois 60510*
[13]*Florida State University, Tallahassee, Florida 32306*
[14]*University of Hawaii, Honolulu, Hawaii 96822*
[15]*University of Illinois at Chicago, Chicago, Illinois 60607*
[16]*Indiana University, Bloomington, Indiana 47405*
[17]*Iowa State University, Ames, Iowa 50011*
[18]*Korea University, Seoul, Korea*
[19]*Kyungsung University, Pusan, Korea*
[20]*Lawrence Berkeley Laboratory and University of California, Berkeley, California 94720*
[21]*University of Maryland, College Park, Maryland 20742*
[22]*University of Michigan, Ann Arbor, Michigan 48109*
[23]*Michigan State University, East Lansing, Michigan 48824*
[24]*Moscow State University, Moscow, Russia*
[25]*University of Nebraska, Lincoln, Nebraska 68588*
[26]*New York University, New York, New York 10003*
[27]*Northeastern University, Boston, Massachusetts 02115*
[28]*Northern Illinois University, DeKalb, Illinois 60115*
[29]*Northwestern University, Evanston, Illinois 60208*
[30]*University of Notre Dame, Notre Dame, Indiana 46556*
[31]*University of Oklahoma, Norman, Oklahoma 73019*
[32]*University of Panjab, Chandigarh 16-00-14, India*
[33]*Institute for High Energy Physics, 142-284 Protvino, Russia*
[34]*Purdue University, West Lafayette, Indiana 47907*
[35]*Rice University, Houston, Texas 77251*
[36]*Universidade Estadual do Rio de Janeiro, Brazil*
[37]*University of Rochester, Rochester, New York 14627*
[38]*CEA, DAPNIA/Service de Physique des Particules, CE-SACLAY, France*
[39]*Seoul National University, Seoul, Korea*
[40]*State University of New York, Stony Brook, New York 11794*
[41]*SSC Laboratory, Dallas, Texas 75237*
[42]*Tata Institute of Fundamental Research, Colaba, Bombay 400005, India*

[43]*University of Texas, Arlington, Texas 76019*
[44]*Texas A&M University, College Station, Texas 77843*
(Received 11 September 1995; revised manuscript received 31 January 1996)

The global topologies of inclusive three- and four-jet events produced in $\overline{pp}$ interactions are described. The three- and four-jet events are selected from data recorded by the D0 detector at the Fermilab Tevatron Collider operating at a center-of-mass energy of $\sqrt{s}=1800$ GeV. The measured, normalized distributions of various topological variables are compared with parton-level predictions of tree-level QCD calculations. The parton-level QCD calculations are found to be in good agreement with the data. The studies also show that the topological distributions of the different subprocesses involving different numbers of quarks are very similar and reproduce the measured distributions well. The parton-shower Monte Carlo generators provide a less satisfactory description of the topologies of the three- and four-jet events. [S0556-2821(96)01611-6]

PACS number(s): 14.65.Ha, 13.85.Ni, 13.85.Qk

INTRODUCTION

The Fermilab Tevatron Collider provides a unique opportunity to study the properties of strong interactions in $\overline{pp}$ collisions at short distances. The hard scattering is described by the theory of perturbative quantum chromodynamics (QCD) [1–3] and has been studied extensively in the last decade [4,5]. Within the context of QCD, the hard process is described as a pointlike scattering between constituent partons (quarks and gluons) of protons and antiprotons. The scattering cross sections can be written in expansions in terms of powers of the strong coupling constant α_s convoluted with parton momentum distributions inside the nucleon. The lowest-order α_s^2 term corresponds to the production of two-parton final states. Terms of order α_s^3 and α_s^4 in the expansion imply the existence of three- and four-parton final states, respectively. Colored partons from the hard scattering evolve via soft quark and gluon radiation and hadronization processes to form observable colorless hadrons, which appear in the detector as localized energy deposits identified as jets. High-energy jets originating from partons in the initial hard scattering process are typically isolated from other collision products. They are expected to preserve the energy and direction of the initial partons, and therefore the topologies of the final jet system are assumed to be directly related to those of the initial parton system.

The cross section and angular distributions for two-jet events have been successfully compared with the predictions of QCD [5,6]. A study of three- and four-jet events allows a test of the validity of the QCD calculations to higher order (α_s^3 or beyond) and a probe of the underlying QCD dynamics. This paper explores the topological distributions of three- and four-jet events. The distributions provide sensitive tests of the QCD matrix element calculations. Topological distributions for the three- and four-jet events have been published previously by the UA1, UA2, and CDF Collaborations [7–10]. However, all of these studies imposed requirements on the topological variables themselves, and therefore significantly reduced the phase space under study. For example, all previous studies excluded the forward region and imposed severe limits on the scaled energy variables. These requirements in effect excluded most of the events from the comparisons. This paper extends these studies to previously untested regions of phase space by removing those requirements and represents the most extensive tests of the topologies of the four-jet events. The measured distributions, without restrictions on the topological variables themselves, are compared with the QCD tree-level matrix element calculations. Unless otherwise specified, all distributions are normalized to unit area. The study shows that the QCD calculations reproduce the data well even in the phase space region unexamined by the previous studies. The predictions from simple phase-space matrix elements are shown as a comparison, and the distributions of QCD subprocesses involving different numbers of quarks are also examined. Finally, the data are compared with the predictions of three parton-shower event generators.

DEFINITION OF TOPOLOGICAL VARIABLES

The topological variables used in this paper are defined in the parton or jet center-of-mass system (c.m.s.). The definitions refer to partons and jets interchangeably. The partons are assumed to be massless and the jet masses are ignored by using the measured jet energies as the magnitudes of jet momenta.

The topological properties of the three-parton final state in the center-of-mass system can be described in terms of six variables. Three of the variables reflect partition of the c.m.s. energy among the three final-state partons. The other three variables define the spatial orientation of the planes containing the three partons. It is convenient to introduce the notation $1+2\rightarrow 3+4+5$ for the three-parton process. Here, numbers 1 and 2 refer to incoming partons while the numbers 3, 4, and 5 label the outgoing partons, ordered in descending c.m.s. energies, i.e., $E_3>E_4>E_5$. The final state parton energy is an obvious choice for the topological variables for the three-parton final state. For simplicity, $E_i(i=3,4,5)$ is often replaced by the scaled variable $x_i(i=3,4,5)$, which is defined by $x_i=2E_i/\sqrt{\hat{s}}$, where $\sqrt{\hat{s}}$ is the center-of-mass energy of the hard scattering process. By definition, $x_3+x_4+x_5=2$. The scaled parton energies x_i and the angles between partons ($\omega_{jk}, j,k=3,4,5$) for the three-parton final state have the relationship

*Visitor from CONICET, Argentina.
†Visitor from IHEP, Beijing, China.
‡Visitor from Universidad de Buenos Aires, Argentina.
§Visitor from Univ. San Francisco de Quito, Ecuador.

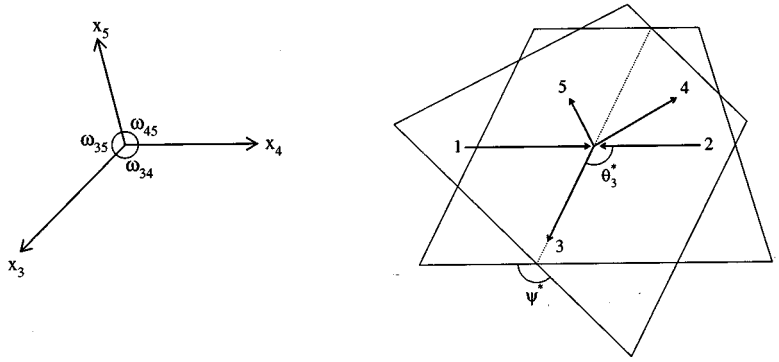

FIG. 1. Illustration of the topological variables x_i, ω_{ij}, θ_3^*, and ψ^* for the three-jet events.

$$x_i=\frac{2\sin\omega_{jk}}{\sin\omega_{34}+\sin\omega_{45}+\sin\omega_{53}}, \tag{1}$$

where $i,j,k=3,4,5$ and $i\neq j\neq k$. Clearly, the internal structure of the three-parton final state is completely determined by any two scaled parton energies. The angles that fix the event orientation can be chosen to be (1) the cosine[1] of the polar angle with respect to the beam ($\cos\theta_3^*$) of parton 3, (2) the azimuthal angle of parton 3 (ϕ_3^*), and (3) the angle between the plane containing partons 1 and 3 and the plane containing partons 4 and 5 (ψ^*) defined by

$$\cos\psi^*=\frac{(\vec{p}_1\times\vec{p}_3)\cdot(\vec{p}_4\times\vec{p}_5)}{|\vec{p}_1\times\vec{p}_3||\vec{p}_4\times\vec{p}_5|}, \tag{2}$$

where $\vec{p}_i$ is the parton momentum. Figure 1 illustrates the definition of the topological variables for the three-parton final state. For unpolarized beams (as at the Tevatron), the ϕ_3^* distribution is uniform. Therefore, only four independent kinematic variables are needed to describe the topological properties of the three-parton final state. In this paper, they are chosen to be x_3, x_5, $\cos\theta_3^*$, and ψ^*.

Another set of interesting variables is the scaled invariant mass of jet pairs:

$$\mu_{ij}=\frac{m_{ij}}{\sqrt{\hat{s}}}\equiv\sqrt{x_ix_j(1-\cos\omega_{ij})/2}, \quad i,j=3,4,5 \text{ and } i\neq j, \tag{3}$$

where m_{ij} is the invariant mass of partons i and j and ω_{ij} is the opening angle between the two partons. The scaled invariant mass (μ_{ij}) is sensitive to the scaled energies of the two partons, the angle between the two partons, and the correlations between these variables. Using dimensionless variables and making comparisons of normalized distributions minimizes the systematic errors due to detector resolution and jet energy scale uncertainty and therefore facilitates comparison between data and theoretical calculation.

The four-parton final state is more complicated. Apart from the c.m.s. energy, eight independent parameters are needed to completely define a four-parton final state in its center-of-mass system. Two of these define the overall event orientation while the other six fix the internal structure of the four-parton system. In contrast to the three-parton final state, there is no simple relationship between the scaled parton energies and the opening angles between partons. Consequently, the choice of topological variables is less obvious in this case. In this paper, variables are defined in a way similar to those investigated for the three-parton final state. The four partons are ordered in descending c.m.s. energy and labeled from 3 to 6. The variables include the scaled energies (x_i, $i=3,\ldots,6$), the cosines of polar angles ($\cos\theta_i^*$, $i=3,\ldots,6$) of the four jets, the cosines of the opening angles between partons ($\cos\omega_{ij}$, $i,j=3,\ldots,6$, and $i\neq j$), and the scaled masses ($\mu_{ij}=m_{ij}/\sqrt{\hat{s}}$, $i,j=3,\ldots,6$ and $i\neq j$) of parton pairs. In addition, two variables characterizing the orientation of event planes are investigated. One of the two variables is the ''Bengtsson-Zerwas'' angle ($\chi_{\rm BZ}$) [11] defined as the angle between the plane containing the two leading jets and the plane containing the two nonleading jets:

$$\cos\chi_{\rm BZ}=\frac{(\vec{p}_3\times\vec{p}_4)\cdot(\vec{p}_5\times\vec{p}_6)}{|\vec{p}_3\times\vec{p}_4||\vec{p}_5\times\vec{p}_6|}. \tag{4}$$

The other variable is the cosine of the ''Nachtmann-Reiter'' angle ($\cos\theta_{\rm NR}$) [12] defined as the angle between the momentum vector differences of the two leading jets and the two nonleading jets:

$$\cos\theta_{\rm NR}=\frac{(\vec{p}_3-\vec{p}_4)\cdot(\vec{p}_5-\vec{p}_6)}{|\vec{p}_3-\vec{p}_4||\vec{p}_5-\vec{p}_6|}. \tag{5}$$

Figure 2 illustrates the definitions of $\chi_{\rm BZ}$ and $\theta_{\rm NR}$ variables. Historically, $\chi_{\rm BZ}$ and $\cos\theta_{\rm NR}$ were proposed for e^+e^- collisions to study gluon self-coupling. Their interpretation in $p\bar{p}$ collisions is more complicated, but the variables can be used as a tool for studying the internal structure of the four-jet events.

THEORETICAL MODEL

The cross section for the production of the n-parton final state $1+2\rightarrow3+\cdots+(n+2)$, in $p\bar{p}$ collisions at a center-of-mass energy $\sqrt{s}$, is described by the expression

$$\sigma_n=\sum_l\int f_1^l(x_1)f_2^l(x_2)|M_l^n|^2\Phi_n dx_1dx_2, \tag{6}$$

[1]Unless otherwise specified, the absolute values of the cosines of polar angles are implied throughout this paper.

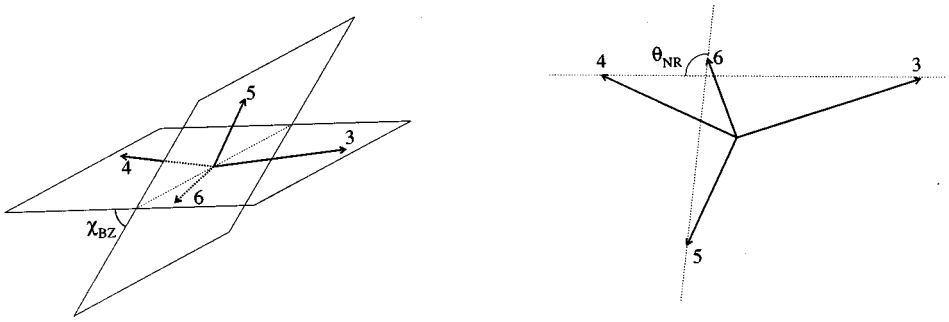

FIG. 2. Illustration of χ_{BZ} and θ_{NR} definitions for the four-jet events.

where the sum runs over all possible $(1+2\rightarrow n)$-parton subprocesses. The functions $f_1^l(x_1)$ and $f_2^l(x_2)$ are the parton density functions of the incoming partons, $|M_l^n|^2$ represents the matrix elements of the subprocess, and Φ_n is the n-body phase space. Theoretically $|M_l^n|^2$ is well behaved if calculated to all orders in the α_s expansion. At present, this calculation is technically not possible and one has to deal with truncated expansion. As a result, $|M_l^n|^2$ diverges when the energy of any final state parton or the angle between any two partons approaches zero. The singularities in $|M_l^n|^2$ cause poles in the topological distributions. In comparison, a phase-space model in which $|M_l^n|^2 \propto 1/\hat{s}^{n-2}$, where $\hat{s}=x_1x_2s$, does not have singularities in the matrix element; therefore, the topology of the model is determined by the phase space Φ_n. In this paper, the distributions from the phase-space model are used as references for the comparisons between the data and QCD.

Presently two approaches for modeling perturbative QCD for multijet production exist. The straightforward method is the matrix element method, in which Feynman diagrams are calculated order by order in α_s. Technical difficulties have limited the calculations to the tree level of the relevant processes. The exact tree-level matrix element calculation for the three-parton final state has been available for some time [13]. The complete tree-level matrix element calculations for up to five final state partons have been recently calculated by Berends, Giele, and Kuijf (BGK) [14] using a Monte Carlo method. The other commonly used approximate calculations are those of Kunszt and Stirling (KS) [15] and of Maxwell [16]. The perturbative QCD calculations have been incorporated into several partonic event generators. The exact tree-level matrix elements calculations for up to five jets are implemented in the NJETS [14] program. PAPAGENO [17] implements an exact matrix element calculation of tree-level contributions for final states with up to three partons and provides KS and Maxwell approximations for up to six partons. These approximations are used in part to speed up the calculations, in view of the complicated exact matrix elements. For the analysis described in this paper, the NJETS program is used to calculate QCD predictions while the PAPAGENO program is used as a cross-check and to calculate distributions from the phase-space model.

The second approach is based on the parton-shower scheme. In this method, the hard scattering begins with two initial outgoing partons. An arbitrary number of partons are then branched off from the two outgoing partons and the two incoming partons (backward evolution) to yield a description for multiparton production, with no explicit upper limit on the number of partons involved. The parton-shower picture is derived within the framework of the leading logarithmic approximation (LLA) [18]. As a result of the approximation, the reliability of the parton shower is expected to decrease as parton multiplicity increases. Many parton-shower Monte Carlo event generators are available. In this paper, HERWIG 5.8 [19], ISAJET 7.13 [20], and PYTHIA 5.6 [21] are used.

DATA SAMPLE

The data used in this analysis were collected with the D0 detector during the 1992–1993 Tevatron run at a center-of-mass energy of 1800 GeV. The D0 detector consists of a central tracking system, a calorimeter, and muon chambers. Jets are measured in the calorimeter, which has a transverse segmentation of $\Delta\eta\times\Delta\phi=0.1\times0.1$. The jet energy resolution is typically 15% at $E_T=50$ GeV and 7% at $E_T=150$ GeV [22]. The jet direction is measured with a resolution of approximately 0.05 in both η and ϕ. With the hermetic and uniform rapidity coverage $(-4.5<\eta<4.5)$ of the calorimeter, the D0 detector is well suited for studying multijet physics. A detailed description of the D0 detector can be found elsewhere [23].

The events used in this study passed hardware (level 1) and software (level 2) energy-cluster-based triggers. In addition, a level 0 hardware trigger required that vertices along the beam line be within 10.5 cm of $z=0$. The level 1 trigger was based on energy deposited in calorimeter towers of size $\Delta\eta\times\Delta\phi=0.2\times0.2$. The events were required to have at least two such towers with transverse energy (E_T) above 7 GeV. The successful candidates were passed to the level 2 trigger, which summed transverse energies of calorimeter towers in a cone of radius $\mathcal{R}[\equiv(\Delta\eta^2+\Delta\phi^2)^{1/2}]=0.7$. The level 2 trigger selected those events with at least one such cone, built around the level 1 trigger tower, with transverse energy above 50 GeV. The total effective luminosity used in this analysis is 1.2 pb^{-1}. The trigger efficiency for events with at least one jet with $E_T>60$ GeV is above 90% [31]. A detailed description of the trigger can be found elsewhere [24].

The off-line reconstruction uses a fixed-cone jet algorithm with $\mathcal{R}=0.7$, similar to the algorithm used in the level 2 trigger. The jet reconstruction begins with seed calorimeter towers of size $\Delta\eta\times\Delta\phi=0.1\times0.1$ containing more than 1 GeV transverse energy. Towers are represented by massless four-momentum vectors with directions given by the tower positions and event vertices. The four-momenta of towers in the cone around the seed tower are summed to form the

four-momentum vector of the jet. The jet direction is then recalculated using tower directions weighted by their transverse energies. The procedure is repeated until the jet axis converges. For two overlapping jets, if either jet shares more than 50% of its transverse energy with the other jet, the two jets are merged. Otherwise, they are split and the shared transverse energy is equally divided between the two jets. The final jet E_T is the sum of the transverse energies of towers within the cone, while the jet direction is determined by the jet four-momentum vector (E,E_x,E_y,E_z), i.e., $\theta=\cos^{-1}(E_z/\sqrt{E_x^2+E_y^2+E_z^2})$, $\phi=\tan^{-1}(E_y/E_x)$, and $\eta=-\ln\tan(\theta/2)$.

The jet energy scale has been calibrated using direct photon candidates by balancing jet E_T against that of the photon candidate. The electromagnetic energy scale was determined by comparing the measured electron pair mass of $Z\rightarrow e^+e^-$ events with the Z mass [25] measured by e^+e^- experiments. The calibration takes into account the effects of out-of-cone particle showering using shower profiles from test beam data as well as the underlying event using events from minimum-bias triggers. Details can be found in Ref. [26].

After energy corrections, jets are required to have E_T greater than 20 GeV and lie within a pseudorapidity range of -3.0 to 3.0. The pseudorapidity is calculated with respect to the event vertex determined from tracks measured by the central tracking detector. Jets passing the above criteria are ordered in decreasing E_T. The E_T of the leading jet must be greater than 60 GeV to reduce possible trigger bias and threshold effects.

Three-jet events are selected by further demanding that there be at least three jets. This leaves about 94 000 events in the sample. The separation $\Delta\mathcal{R}$ between jets is required to be greater than 1.4, which is twice the cone size used, to avoid systematic uncertainty associated with the merging or splitting of the cone jet algorithm. This requirement removes events with overlapping jets and therefore ensures good jet energy and direction measurements. Approximately 70% of the events pass this requirement. The invariant mass distribution of the three highest E_T jets is shown in Fig. 3. Also shown is the distribution from the exact tree-level calculations of perturbative QCD after the detector simulation described below. The overall agreement between the data and QCD distributions is good with the exception of the low-mass region, where the threshold and resolution effects are important. To reduce possible bias in this region, the invariant mass of the three leading jets is required to be above 200 GeV/c^2. After all selection criteria, a sample of about 46 000 three-jet events remains. The surviving events are then transformed to the c.m.s. frame of the three leading jets. Any other jets in the event are ignored. The jets are reordered in descending energy in their c.m.s. system. The topological variables (x_3, x_4, $\cos\theta_3^*$, and ψ^*) are calculated. Unlike previous studies by other experiments, no requirements on these topological variables are imposed. If the topological requirements similar to those in Ref. [8] were imposed, the three-jet event sample would be reduced by more than a factor of 10.

Four-jet events are selected in a similar manner. Events are required to have at least four jets, which results in a data sample of 19 000 events. The $\Delta\mathcal{R}$ between any jet pair is required to be greater than 1.4, reducing the data sample to about 8400 events. To reduce potential bias at low mass while keeping most of the four-jet events, the minimum invariant mass of the leading four jets is kept at 200 GeV/c^2. The mass distribution before this requirement is applied is shown in Fig. 3. A total of 8100 events remains in the four-jet event sample. The four leading jets of the remaining events are boosted to their center-of-mass system, and are ordered in decreasing energy. Additional jets, if present, are ignored. The topological variables are calculated using the four boosted momentum vectors after ordering in decreasing energy. No requirements on the topological variables are imposed.

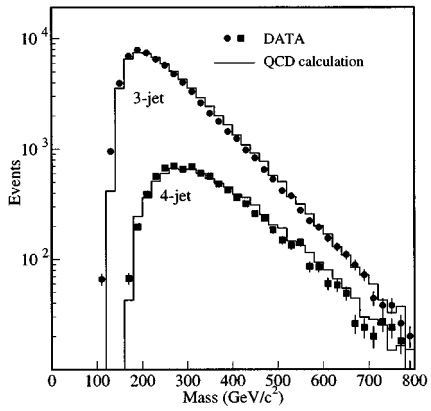

FIG. 3. The mass distributions of the selected three- and four-jet events before the mass requirement. The QCD matrix element calculations are subjected to the detector simulation and are normalized to the number of events in the data.

PREDICTIONS OF THEORETICAL MODELS

The partonic event generator NJETS is used to calculate the exact tree-level QCD distributions. The PAPAGENO program is used to calculate the distributions of the phase-space model and the KS approximation. Unless otherwise specified, the parton distribution function used in the calculations is MRS (BCDMS fit) [27] for both NJETS and PAPAGENO. The QCD scale parameter is set to 200 MeV and the renormalization scales are set to the average transverse momentum of the outgoing partons for both matrix elements and parton distribution functions. The outgoing partons are analyzed as if they were observed jets and the selection criteria described above are applied to select three- and four-jet events.

To study the sensitivity to the choice of parton distribution function, the topological distributions of QCD calculations with different parton distribution functions are compared. For NJETS, the comparisons are made between MRS [27] and EHLQ [28] parton distribution functions. For PAPAGENO the parton distribution functions of MRS [27] and Morfin and Tung [29] are employed. Although the total three- and four-jet cross sections vary by as much as 30% for different parton distribution functions, the normalized topological distributions are found to be relatively insensitive to the choice. On average, the variation is about 4%.

As an example, the fractional difference in the NJETS calculations using the two different parton distribution functions is shown in Fig. 4(a) as dashed line for the x_3 variable of the

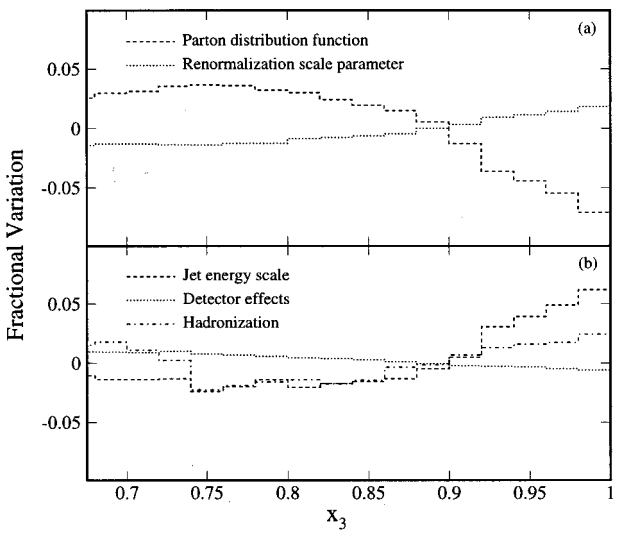

FIG. 4. The fractional variations of the x_3 variable of the three-jet events for the different systematic sources discussed in the text for (a) the QCD calculations and (b) the data. The x_3 distribution is shown in Fig. 5(a) for both the data and the QCD calculation. The variations in different bins are strongly correlated due to the fixed normalization of the distribution.

three-jet events. The x_3 distribution from the NJETS calculations is shown in Fig. 5(a). Because of the unit area normalization of the distributions, the variations in different bins are correlated.

The dependences on the renormalization scale are investigated using the PAPAGENO program. The distributions for the renormalization scales of (1) the average transverse momentum, (2) one-half the average value of transverse momentum, and (3) the total transverse energy are compared. Despite large differences (as much as 60%) in the total production cross sections, the differences between normalized distributions are very small, typically less than 2%. Figure 4(a) (dotted line) shows the bin-by-bin uncertainty of the x_3 distribution of the three-jet events due to the uncertainty in the renormalization scale parameter.

In the following comparison with the data, the variations in the QCD calculations using different normalization scale parameters and parton distribution functions are calculated on a bin-by-bin basis. The uncertainty in the QCD calculations is taken as the sum of these variations in quadrature.

Both NJETS and PAPAGENO incorporate tree-level calculations for three- and four-parton final states. The effect on the normalized distributions due to higher-order loop corrections is expected to be small in the phase-space region relevant to the analyses described in this paper [30]. Although both Monte Carlo programs generate exclusive events, the three or four jets of the generated events predict the behavior of the leading three or four jets of an inclusive data sample [30]. Therefore the data distributions based on the inclusive samples are compared with QCD calculations from exclusive final states in this paper.

UNCERTAINTIES OF THE MEASURED TOPOLOGICAL DISTRIBUTIONS

The measured distributions of topological variables are corrected for detector effects (trigger efficiency and detector acceptance and resolutions) and hadronization effects before they are compared with the parton-level QCD calculations. Most of these corrections and their uncertainties are minimized by normalizing the distributions to unit area and by selection requirements. In the following, residual uncertainties are discussed.

The nonuniformity of the detector acceptance and of the trigger efficiency in the topological variables and the detector energy resolution and angular resolution have direct effects on the measured distributions. These effects are estimated using a fast detector simulation program [31] which takes into account the detector energy and angular resolution and the trigger efficiency as functions of the pseudorapidity and the transverse energy of jets. The bin-by-bin correction

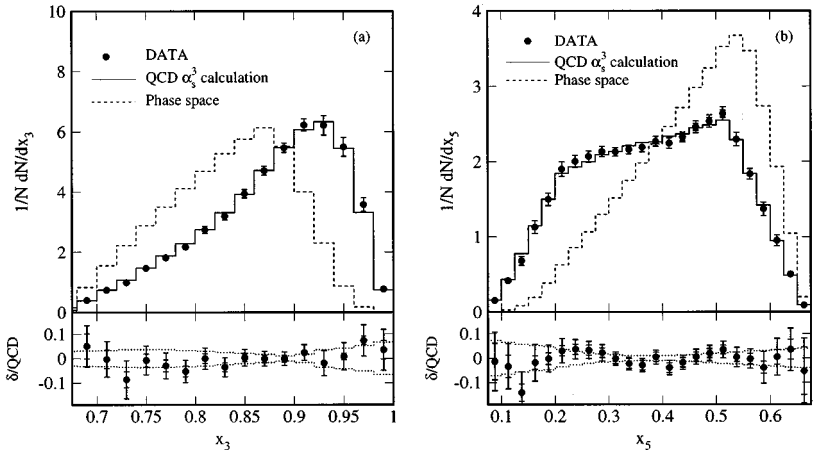

FIG. 5. The scaled energy distributions of (a) x_3 and (b) x_5 for three-jet events in their center-of-mass system. The statistical errors are represented by the inner error bars while the total errors (with the statistical and systematic errors added in quadrature) are represented by the outer error bars. All distributions are normalized to unit area. The bottom plot shows the fractional difference of the data from the exact tree-level QCD calculation. The dotted lines show the uncertainty of the QCD calculations estimated by varying the normalization scale parameter and using different parton distribution function in the calculations as discussed in the text. The bin-by-bin systematic variations of the x_3 variable for data and the QCD calculations are shown in Fig. 4. The data are also listed in Table I.

TABLE I. The measured x_3 and x_5 distributions with their statistical errors for the three-jet events. The errors include both the statistical and systematic errors.

x_3	$1/NdN/dx_3$	x_5	$1/NdN/dx_5$
0.66–0.68	0.07±0.01	0.075–0.100	0.15±0.02
0.68–0.70	0.40±0.03	0.100–0.125	0.42±0.04
0.70–0.72	0.74±0.05	0.125–0.150	0.68±0.06
0.72–0.74	0.99±0.08	0.150–0.175	1.13±0.09
0.74–0.76	1.47±0.09	0.175–0.200	1.50±0.08
0.76–0.78	1.82±0.10	0.200–0.225	1.90±0.09
0.78–0.80	2.18±0.10	0.225–0.250	2.00±0.08
0.80–0.82	2.74±0.12	0.250–0.275	2.07±0.07
0.82–0.84	3.19±0.12	0.275–0.300	2.13±0.07
0.84–0.86	3.94±0.14	0.300–0.325	2.13±0.06
0.86–0.88	4.71±0.14	0.325–0.350	2.16±0.06
0.88–0.90	5.47±0.16	0.350–0.375	2.19±0.06
0.90–0.92	6.22±0.21	0.375–0.400	2.27±0.06
0.92–0.94	6.22±0.32	0.400–0.425	2.24±0.07
0.94–0.96	5.50±0.31	0.425–0.450	2.32±0.07
0.96–0.98	3.57±0.23	0.450–0.475	2.46±0.08
0.98–1.00	0.77±0.06	0.475–0.500	2.54±0.08
		0.500–0.525	2.64±0.09
		0.525–0.550	2.30±0.09
		0.550–0.575	1.84±0.07
		0.575–0.600	1.37±0.09
		0.600–0.625	0.95±0.07
		0.625–0.650	0.50±0.04
		0.650–0.675	0.09±0.01

factors applied are flat within 5%. The uncertainties of the correction factors are estimated by varying the trigger efficiency and the detector resolutions within their errors. As an example, the bin-by-bin fractional variation of the x_3 distribution of the three-jet events due to the uncertainty of the detector corrections is shown in Fig. 4(b) as a dotted line. The variations are very small ($\sim$1%) and are correlated from bin to bin due to the normalization.

After corrections for the detector effects, the measured distributions are further corrected for hadronization effects which are determined using the HERWIG event generator. The parton-level distributions for three- and four-jet events are compared with the distributions at the particle level. Partons are defined as those quarks and gluons after the parton showering and before hadronization. The differences between the distributions before and after hadronization are found to be small, typically less than 4%. The uncertainties of the correction factors are investigated using the HERWIG and the PYTHIA event generators. The differences in the correction factors between the two event generators are assigned as systematic uncertainties. Figure 4(b) (dot-dashed line) shows the bin-by-bin fractional uncertainty of the x_3 distribution of the three-jet events due to the uncertainty of the hadronization corrections. The uncertainties are less than 2% for most of the bins. Again, the bin-by-bin uncertainties are strongly correlated since the x_3 distribution is normalized to unit area.

Another systematic uncertainty of the measured distributions is the uncertainty of the jet energy scale. However, the topological variables have a weak dependence on the energy scale since only the scaled energies and directions of the jets are used. Nevertheless, the event selection criteria, such as E_T and invariant mass requirements, are susceptible to the uncertainty in energy scale error. The possible distortion of the measured topological variables due to the uncertainty in the energy scale is studied by varying the energy calibration constants within their nominal errors which take into account the pseudorapidity-dependent systematic effect of the energy scale. The selection procedure described above is repeated for the events calibrated with these modified constants. On average, the variations in the measured topological variables are about 3%. The small variation is in part due to the fact that the topological distributions change slowly with the jet E_T and the invariant mass of the jet system. The fractional variation in the x_3 distribution of the three-jet events due to the uncertainty in the jet energy scale is shown in Fig. 4(b) as a dashed line.

In the following, the measured topological distributions after being corrected for detector and hadronization effects are compared with the QCD tree-level calculations at the parton level. The variations on the measured distributions due to the uncertainties of the correction factors and the uncertainty of the jet energy scale are calculated bin by bin. These variations are added in quadrature bin by bin and the sum is assigned as systematic uncertainty of the measurement for each bin. Finally, we note that changing the jet separation requirement $\Delta\mathcal{R}$ from 1.4 to 1.0 does not change the degree of agreement between the data and QCD calculations.

TOPOLOGIES OF THREE-JET EVENTS

Figure 5 and Table I show the measured x_3 and x_5 distributions for the final selection of three-jet events. The statistical errors are represented by the inner error bars while the outer error bars represent the statistical and bin-by-bin systematic errors added in quadrature. The three jets are labeled in order of decreasing energy in their c.m.s. frame. The average values of x_3 and x_5 are 0.88 and 0.39, respectively. The data are compared with the predicted distributions of the exact QCD tree-level calculations and the expectations from the phase-space model. The QCD calculations reproduce the measured distributions well for the entire range. Unlike the predictions of the phase-space model, the data heavily populate the high x_3 region and have significant contributions at low x_5 values, a characteristic of gluon radiation. The decrease in x_3 distributions at high x_3 values is due to the $\Delta\mathcal{R}$ requirement in the event selection. The bottom plot shows the fractional difference between the data and the QCD predictions with dotted lines indicating the uncertainty of the QCD predictions using different normalization scale parameters and different parton distribution functions discussed above. The bin-by-bin variations of the x_3 variable for both data and the QCD calculations from the different systematic sources discussed above are shown in Fig. 4.

The $\cos\theta_3^*$ distribution is shown in Fig. 6(a). As in the angular distribution of two-jet events, an angular dependence characteristic of Rutherford t-channel scattering is unmistakable. The large angular coverage of the D0 calorimeter allows the analysis to cover the entire $\cos\theta_3^*$ range, extending the study into a previously untested region of phase space.

TABLE II. The measured $\cos\theta_3^*$ and ψ^* distributions for the three-jet events. The errors include both statistical and systematic errors.

$\cos\theta_3^*$	$1/NdN/d\cos\theta_3^*$	ψ^*	$1/NdN/d\psi^*$
0.00–0.05	0.15±0.01	0.0–10.0	0.0074±0.0002
0.05–0.10	0.17±0.01	10.0–20.0	0.0079±0.0002
0.10–0.15	0.17±0.01	20.0–30.0	0.0078±0.0002
0.15–0.20	0.18±0.01	30.0–40.0	0.0068±0.0002
0.20–0.25	0.19±0.01	40.0–50.0	0.0056±0.0002
0.25–0.30	0.19±0.01	50.0–60.0	0.0044±0.0002
0.30–0.35	0.25±0.01	60.0–70.0	0.0037±0.0001
0.35–0.40	0.26±0.01	70.0–80.0	0.0032±0.0001
0.40–0.45	0.28±0.02	80.0–90.0	0.0032±0.0001
0.45–0.50	0.35±0.02	90.0–100.0	0.0031±0.0001
0.50–0.55	0.41±0.02	100.0–110.0	0.0033±0.0001
0.55–0.60	0.53±0.02	110.0–120.0	0.0038±0.0001
0.60–0.65	0.66±0.02	120.0–130.0	0.0044±0.0001
0.65–0.70	0.92±0.03	130.0–140.0	0.0055±0.0002
0.70–0.75	1.20±0.04	140.0–150.0	0.0069±0.0002
0.75–0.80	1.68±0.04	150.0–160.0	0.0080±0.0002
0.80–0.85	2.16±0.05	160.0–170.0	0.0079±0.0002
0.85–0.90	2.78±0.06	170.0–180.0	0.0073±0.0002
0.90–0.95	3.67±0.08		
0.95–1.00	3.80±0.09		

As is evident in the figure, the data are well reproduced by the predictions of the exact QCD tree-level calculations over the entire range of $\cos\theta_3^*$. The phase-space distribution is mostly flat with high-$\cos\theta_3^*$ bins suppressed as a result of the pseudorapidity requirement in the event selection. The depletion in the data and the QCD calculations is compensated by a large cross section in this region and therefore is less visible. The measured ψ^* distribution is shown in Fig. 6(b) together with the results of the exact QCD tree-level calculation and of the phase-space model. The phase-space distribution shows depletions at small and large ψ^* angles, an effect of the event selection. However, the data and the QCD distributions are enhanced in these regions because of initial-state radiation in which one of the two nonleading jets is close to the beam line. As in the case of the x_3, x_5, and $\cos\theta_3^*$ distributions, the overall agreement between data and the QCD tree-level calculations is very good.

The scaled mass distributions are sensitive to the jet energies, the opening angles between jets, and the correlations between these quantities. The measured μ_{34},μ_{35}, and μ_{45} distributions for the three-jet event sample are compared with the exact QCD predictions in Fig. 7. The QCD predictions agree with the data well, while the differences between the data and the phase-space model are large. We also note that some systematic shift in μ_{35} and μ_{45} distributions is clearly visible.

We note that the KS approximate QCD calculations are essentially identical to the exact tree-level QCD calculations for the topological variables studied above. This implies that the topological distributions are insensitive to the approximation made in the KS calculations. Finally, we also note that compared with an earlier study [8] of the topologies of the three-jet events, the $\cos\theta_3^*$ region studied has been expanded from 0.8 to 1.0, the x_3 upper limit from 0.9 to 1.0, and the ψ^* range from $20°<\psi^*<160°$ to $0°\leqslant\psi^*\leqslant180°$ for a minimum three-jet invariant mass of 200 GeV/c^2. The ex-

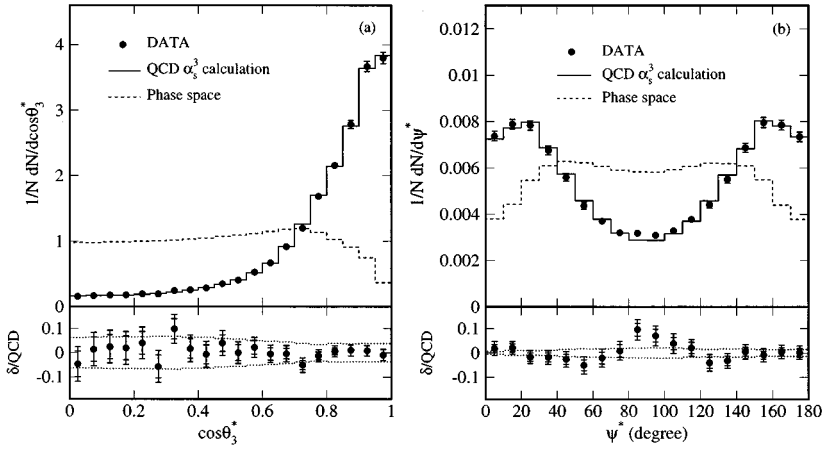

FIG. 6. The distributions for the three-jet events of (a) the cosine of the leading jet polar angle and (b) the angle ψ^* (defined in the text) in their center-of-mass system. The bottom plots show fractional differences between the data and QCD. The dotted lines represent the uncertainty of the QCD calculations described in the text. The data are also listed in Table II.

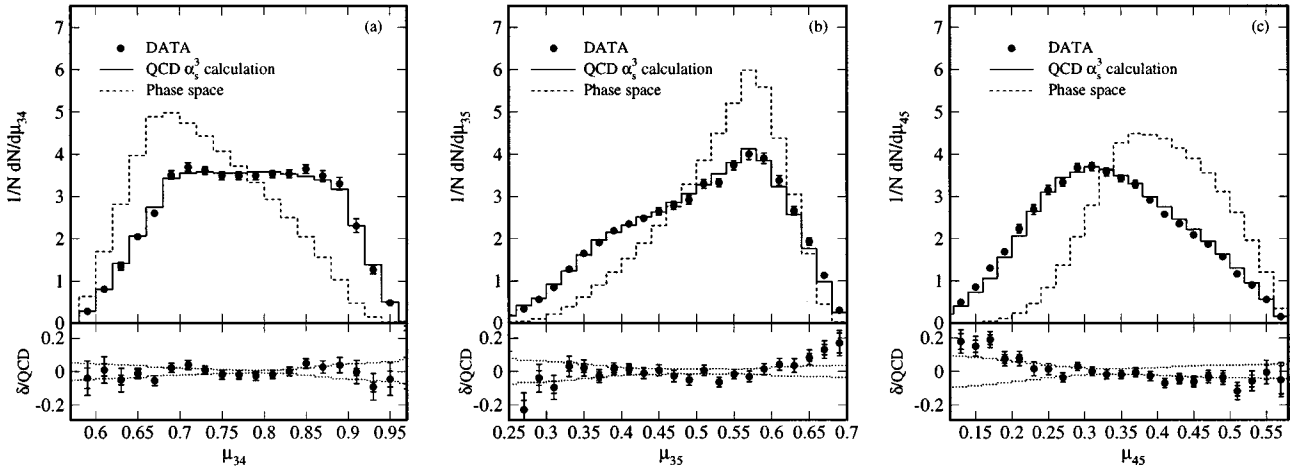

FIG. 7. The scaled mass distributions of (a) μ_{34}, (b) μ_{35}, and (c) μ_{45} for the three-jet events in their center-of-mass system. The bottom plots show fractional differences between the data and QCD. The dotted lines represent the uncertainty of the QCD calculations described in the text. The data are also listed in Table III.

tension of the phase space dramatically increases number of events under study since the cross section peaks strongly in these regions of phase space.

TOPOLOGIES OF FOUR-JET EVENTS

The four measured energy fractions of four-jet events are shown in Fig. 8 and also listed in Table IV. The inner error bars represent the statistical errors while the outer error bars represent the statistical and bin-by-bin systematic errors added in quadrature. The four jets are labeled in order of decreasing energy in their center-of-mass system. Although four scaled energy variables are shown, only three of these are independent. The other is fixed by the condition $\Sigma_i x_i = 2$. The measured mean values of the four energy fractions are 0.76, 0.61, 0.39, and 0.24. The QCD predictions of the exact tree-level calculations are represented by the solid curves and are in an excellent agreement with the data for all

TABLE III. The measured μ_{34}, μ_{35}, and μ_{45} distributions for the three-jet events. The errors include both statistical and systematic errors.

μ_{34}	$1/NdN/d\mu_{34}$	μ_{35}	$1/NdN/d\mu_{35}$	μ_{45}	$1/NdN/d\mu_{45}$
0.58–0.60	0.28±0.03	0.22–0.24	0.10±0.01	0.08–0.10	0.09±0.01
0.60–0.62	0.81±0.06	0.24–0.26	0.20±0.02	0.10–0.12	0.26±0.02
0.62–0.64	1.35±0.09	0.26–0.28	0.34±0.03	0.12–0.14	0.49±0.03
0.64–0.66	2.04±0.06	0.28–0.30	0.57±0.05	0.14–0.16	0.86±0.05
0.66–0.68	2.60±0.08	0.30–0.32	0.84±0.06	0.16–0.18	1.31±0.06
0.68–0.70	3.51±0.10	0.32–0.34	1.28±0.08	0.18–0.20	1.69±0.07
0.70–0.72	3.70±0.10	0.34–0.36	1.65±0.08	0.20–0.22	2.24±0.10
0.72–0.74	3.61±0.09	0.36–0.38	1.91±0.07	0.22–0.24	2.69±0.11
0.74–0.76	3.49±0.09	0.38–0.40	2.19±0.08	0.24–0.26	3.15±0.11
0.76–0.78	3.49±0.09	0.40–0.42	2.35±0.07	0.26–0.28	3.33±0.09
0.78–0.80	3.49±0.10	0.42–0.44	2.49±0.08	0.28–0.30	3.69±0.09
0.80–0.82	3.53±0.09	0.44–0.46	2.65±0.09	0.30–0.32	3.71±0.10
0.82–0.84	3.54±0.09	0.46–0.48	2.78±0.10	0.32–0.34	3.58±0.10
0.84–0.86	3.65±0.10	0.48–0.50	2.92±0.10	0.34–0.36	3.43±0.08
0.86–0.88	3.49±0.13	0.50–0.52	3.30±0.10	0.36–0.38	3.29±0.09
0.88–0.90	3.30±0.15	0.52–0.54	3.33±0.10	0.38–0.40	2.91±0.08
0.90–0.92	2.31±0.16	0.54–0.56	3.74±0.11	0.40–0.42	2.57±0.07
0.92–0.94	1.27±0.10	0.56–0.58	4.01±0.13	0.42–0.44	2.36±0.07
0.94–0.96	0.48±0.05	0.58–0.60	3.91±0.13	0.44–0.46	2.09±0.07
		0.60–0.62	3.38±0.12	0.46–0.48	1.88±0.07
		0.62–0.64	2.66±0.11	0.48–0.50	1.57±0.06
		0.64–0.66	1.93±0.09	0.50–0.52	1.16±0.06
		0.66–0.68	1.13±0.06	0.52–0.54	0.90±0.05
		0.68–0.70	0.30±0.02	0.54–0.56	0.56±0.04
				0.56–0.58	0.15±0.02

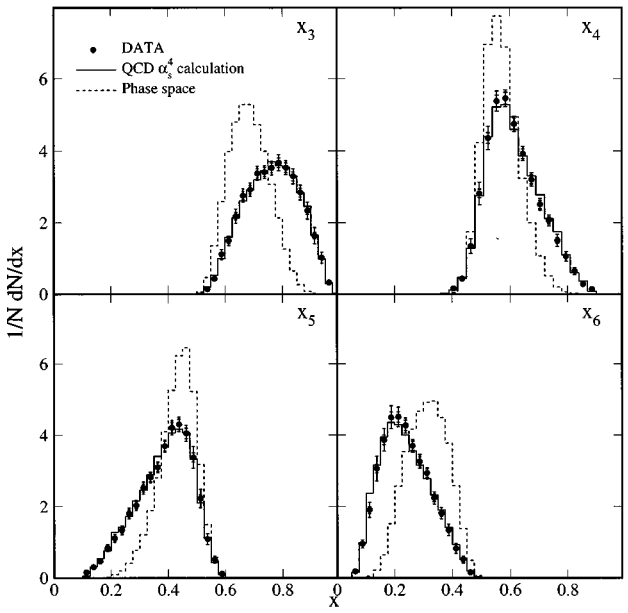

FIG. 8. The jet energy fraction distributions for the four-jet events in their center-of-mass system. All distributions are normalized to unit area. The statistical errors are represented by the inner error bars while the total errors (with the statistical and systematic errors added in quadrature) are represented by the outer error bars. The data are also listed in Table IV.

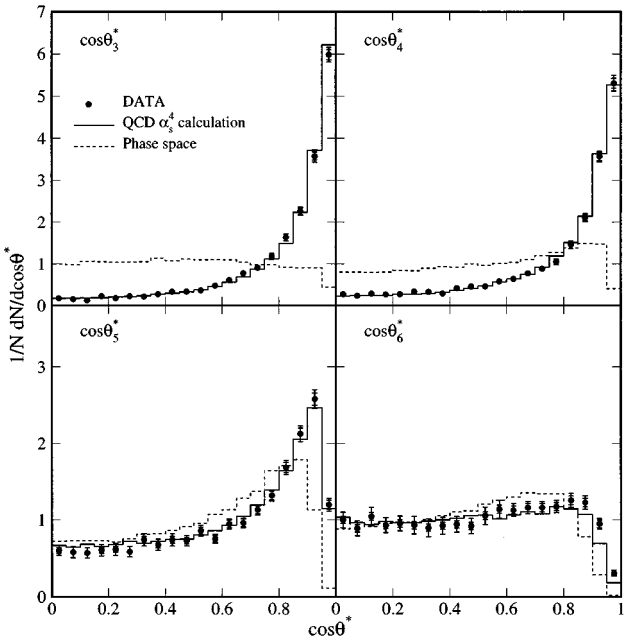

FIG. 9. The distributions of jet polar angle for the four-jet events in their center-of-mass system. The statistical and total errors are represented by the inner and outer error bars, respectively. The data are also listed in Table V.

four variables. As in the three-jet case, the distributions from the phase-space model do not reproduce the data. The fractional differences between the data and QCD are very similar to those of the three-jet events and are not shown for simplicity.

The cosines of the four polar angles of the four-jet events in their center-of-mass system are compared with QCD calculations in Fig. 9 for the entire range. While the two leading jets tend to be in the forward region, the cosine distribution of the least energetic jet is essentially flat, because the jet separation requirement in the event selection favors events with other jets in the central region. Although small differences between the data and the QCD calculations are visible, the overall agreement is good. Despite the large differences between the data and the phase-space model in $\cos\theta_3^*$ and

TABLE IV. The measured jet energy fraction distributions for the four-jet events in their center-of-mass system. The errors include both statistical and systematic errors.

x_3	$1/NdN/dx_3$	x_4	$1/NdN/dx_4$	x_5	$1/NdN/dx_5$	x_6	$1/NdN/dx_6$
0.525–0.550	0.14±0.03	0.39–0.42	0.13±0.03	0.100–0.125	0.15±0.03	0.050–0.075	0.18±0.04
0.550–0.575	0.43±0.08	0.42–0.45	0.36±0.06	0.125–0.150	0.30±0.04	0.075–0.100	0.95±0.11
0.575–0.600	1.11±0.14	0.45–0.48	1.12±0.17	0.150–0.175	0.46±0.06	0.100–0.125	1.90±0.21
0.600–0.625	1.49±0.13	0.48–0.51	2.34±0.26	0.175–0.200	0.83±0.09	0.125–0.150	3.06±0.35
0.625–0.650	2.18±0.20	0.51–0.54	3.63±0.27	0.200–0.225	1.11±0.11	0.150–0.175	3.86±0.32
0.650–0.675	2.75±0.19	0.54–0.57	4.48±0.24	0.225–0.250	1.34±0.13	0.175–0.200	4.50±0.32
0.675–0.700	2.92±0.18	0.57–0.60	4.55±0.19	0.250–0.275	1.80±0.15	0.200–0.225	4.51±0.28
0.700–0.725	3.37±0.19	0.60–0.63	3.96±0.18	0.275–0.300	2.03±0.15	0.225–0.250	4.27±0.21
0.725–0.750	3.41±0.18	0.63–0.66	3.27±0.16	0.300–0.325	2.51±0.17	0.250–0.275	3.70±0.19
0.750–0.775	3.52±0.19	0.66–0.69	2.67±0.15	0.325–0.350	2.81±0.15	0.275–0.300	3.26±0.19
0.775–0.800	3.67±0.22	0.69–0.72	2.09±0.14	0.350–0.375	3.10±0.16	0.300–0.325	2.93±0.16
0.800–0.825	3.53±0.19	0.72–0.75	1.72±0.13	0.375–0.400	3.69±0.18	0.325–0.350	2.23±0.17
0.825–0.850	3.29±0.21	0.75–0.78	1.25±0.14	0.400–0.425	4.21±0.20	0.350–0.375	1.81±0.16
0.850–0.875	2.84±0.21	0.78–0.81	0.88±0.11	0.425–0.450	4.30±0.20	0.375–0.400	1.34±0.17
0.875–0.900	2.33±0.24	0.81–0.84	0.54±0.08	0.450–0.475	4.05±0.23	0.400–0.425	0.82±0.14
0.900–0.925	1.63±0.23	0.84–0.87	0.23±0.05	0.475–0.500	3.37±0.30	0.425–0.450	0.52±0.10
0.925–0.950	1.02±0.16	0.87–0.90	0.12±0.03	0.500–0.525	2.22±0.26	0.450–0.475	0.15±0.04
0.950–0.975	0.32±0.07			0.525–0.550	1.08±0.15		
				0.550–0.575	0.51±0.10		
				0.575–0.600	0.11±0.03		

TABLE V. The measured jet cosine distributions for the four-jet events in their center-of-mass system. The errors include both statistical and systematic errors.

$\cos\theta_i^*$	$1/NdN/d\cos\theta_3^*$	$1/NdN/d\cos\theta_4^*$	$1/NdN/d\cos\theta_5^*$	$1/NdN/d\cos\theta_6^*$
0.00–0.05	0.18±0.03	0.27±0.04	0.60±0.06	1.00±0.10
0.05–0.10	0.16±0.03	0.24±0.04	0.58±0.07	0.89±0.10
0.10–0.15	0.12±0.02	0.29±0.04	0.57±0.07	1.05±0.12
0.15–0.20	0.22±0.04	0.27±0.03	0.60±0.08	0.93±0.10
0.20–0.25	0.18±0.03	0.27±0.04	0.62±0.08	0.95±0.10
0.25–0.30	0.22±0.04	0.33±0.04	0.59±0.07	0.93±0.11
0.30–0.35	0.22±0.03	0.33±0.04	0.74±0.08	0.90±0.11
0.35–0.40	0.27±0.04	0.29±0.04	0.68±0.07	0.92±0.11
0.40–0.45	0.34±0.04	0.42±0.05	0.74±0.08	0.94±0.10
0.45–0.50	0.34±0.04	0.46±0.05	0.73±0.07	0.92±0.10
0.50–0.55	0.37±0.05	0.46±0.06	0.86±0.07	1.05±0.11
0.55–0.60	0.48±0.05	0.58±0.06	0.75±0.06	1.14±0.12
0.60–0.65	0.61±0.05	0.64±0.06	0.95±0.07	1.13±0.09
0.65–0.70	0.77±0.06	0.77±0.06	0.96±0.06	1.16±0.08
0.70–0.75	0.90±0.06	0.88±0.06	1.13±0.07	1.16±0.08
0.75–0.80	1.18±0.07	1.05±0.07	1.32±0.07	1.18±0.08
0.80–0.85	1.63±0.08	1.46±0.09	1.68±0.09	1.26±0.09
0.85–0.90	2.26±0.10	2.11±0.10	2.13±0.10	1.23±0.09
0.90–0.95	3.58±0.15	3.56±0.13	2.58±0.12	0.95±0.07
0.95–1.00	5.98±0.17	5.31±0.19	1.20±0.08	0.31±0.04

$\cos\theta_4^*$ distributions, the differences in the other two distributions are relatively small.

The internal event structure can be further understood by examining the opening angles between jets. Figure 10 shows the distributions of the space angle between all possible jet pairs of the four-jet events in their center-of-mass system. While the two leading jets are mostly back to back, the angles between other jet pairs are distributed widely. The depletion in the regions where $\cos\omega_{ij}\rightarrow 1.0$ is again due to the $\Delta\mathcal{R}$ requirement in the event selection. The structures of the data distributions are well described by the QCD predictions.

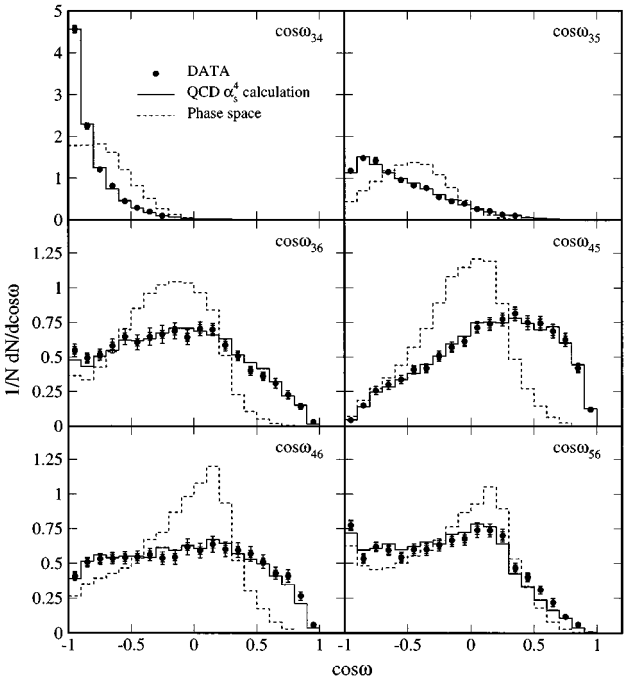

FIG. 10. Distributions of the space angle between jet pairs for the four-jet events in their center-of-mass system. The statistical and total errors are represented by the inner and outer error bars, respectively. The data are also listed in Table VI.

Figure 11 shows the scaled mass distributions of jet pairs of the four-jet events for both data and the QCD calculations. The average scaled mass is 0.65 for the two leading jets and is 0.23 for the two nonleading jets. The QCD calculations agree with the data well. Distributions of the phase-space model are generally too narrow and fail to reproduce the data distributions.

Figure 12 compares the measured $\chi_{\rm BZ}$ and $\cos\theta_{\rm NR}$ distributions with the predictions of the exact tree-level QCD calculations as well as those from the phase-space model. The agreement between the data and QCD is generally good and the differences between the data and the phase-space model are large. Although the jet separation requirement in the event selection favors large $\chi_{\rm BZ}$, the data and the QCD distributions have significant contributions in the small-$\chi_{\rm BZ}$ region, which corresponds to a planar topology of the four jets. In contrast, the phase-space distribution is highly suppressed in this region. The $\cos\theta_{\rm NR}$ distributions for the data and QCD are essentially flat while the phase-space model peaks strongly as $\cos\theta_{\rm NR}$ approaches zero.

For the four-jet events as was the case for the three-jet events, the normalized distributions from the KS approximate QCD calculations agree well with the data.

COMPARISON OF QCD SUBPROCESSES

At the parton level, five and six partons (including the two initial partons) are involved in the three- and four-jet processes, respectively. It is difficult, if not impossible, to label

TABLE VI. The measured distribution of the cosine of space angles between pairs of jets for the four-jet events in their center-of-mass system. The errors include both statistical and systematic errors.

$\cos\omega_{ij}$	$1/NdN/d\cos\omega_{34}$	$1/NdN/d\cos\omega_{35}$	$1/NdN/d\cos\omega_{36}$	$1/NdN/d\cos\omega_{45}$	$1/NdN/d\cos\omega_{46}$	$1/NdN/d\cos\omega_{56}$
−1.0 to −0.9	4.565±0.092	1.180±0.062	0.548±0.046	0.043±0.009	0.409±0.030	0.774±0.039
−0.9 to −0.8	2.250±0.071	1.484±0.064	0.493±0.036	0.151±0.020	0.508±0.035	0.534±0.035
−0.8 to −0.7	1.207±0.051	1.421±0.077	0.516±0.040	0.258±0.029	0.533±0.039	0.621±0.034
−0.7 to −0.6	0.815±0.045	1.148±0.059	0.581±0.050	0.299±0.031	0.536±0.040	0.594±0.035
−0.6 to −0.5	0.450±0.037	0.956±0.053	0.647±0.057	0.338±0.030	0.540±0.043	0.544±0.038
−0.5 to −0.4	0.286±0.032	0.826±0.048	0.606±0.055	0.408±0.032	0.544±0.045	0.599±0.041
−0.4 to −0.3	0.194±0.029	0.768±0.045	0.647±0.062	0.420±0.032	0.563±0.043	0.600±0.042
−0.3 to −0.2	0.096±0.019	0.552±0.038	0.663±0.064	0.507±0.037	0.537±0.045	0.633±0.044
−0.2 to −0.1	0.057±0.014	0.444±0.034	0.688±0.059	0.572±0.038	0.545±0.052	0.665±0.044
−0.1–0.0	0.026±0.008	0.389±0.036	0.643±0.054	0.615±0.038	0.619±0.057	0.676±0.047
0.0–0.1	0.021±0.007	0.263±0.029	0.704±0.050	0.714±0.042	0.592±0.053	0.739±0.053
0.1–0.2	0.022±0.008	0.211±0.026	0.698±0.045	0.740±0.044	0.637±0.058	0.737±0.048
0.2–0.3	0.008±0.004	0.128±0.021	0.586±0.041	0.773±0.047	0.601±0.052	0.699±0.045
0.3–0.4		0.101±0.019	0.508±0.036	0.814±0.048	0.594±0.054	0.465±0.037
0.4–0.5		0.063±0.014	0.401±0.032	0.750±0.050	0.568±0.053	0.401±0.032
0.5–0.6		0.037±0.010	0.361±0.031	0.744±0.050	0.512±0.049	0.309±0.029
0.6–0.7		0.022±0.007	0.309±0.036	0.688±0.049	0.429±0.043	0.219±0.028
0.7–0.8		0.005±0.003	0.228±0.029	0.626±0.048	0.409±0.044	0.118±0.017
0.8–0.9		0.002±0.002	0.143±0.021	0.421±0.032	0.266±0.031	0.060±0.011
0.9–1.0			0.031±0.009	0.121±0.014	0.058±0.010	0.011±0.004

quark or gluon jets in the data. However, with Monte Carlo event generators, the three-jet cross section can be broken into three subprocesses involving different numbers of quarks among the initial- or final-state partons: (1) zero-quark, (2) two-quark, and (3) four-quark. The predicted fractional contributions by NJETS to the total three-jet cross section for the selection criteria described above are 32.9%, 50.8%, and 16.2% for zero-quark, two-quark, and four-quark subprocesses, respectively. Similarly, the four-jet process can be divided into (1) zero-quark (29.4%), (2) two-quark (49.6%), (3) four-quark (20.2%), and (4) six-quark (0.7%) subprocesses.

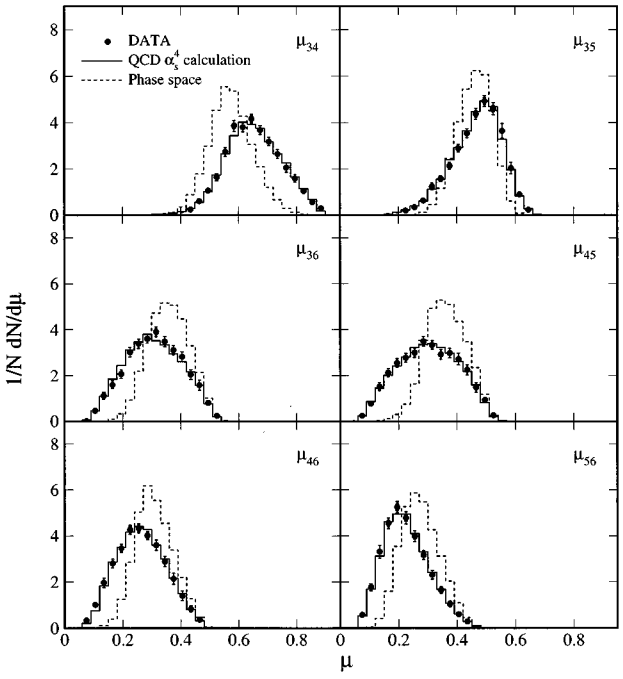

FIG. 11. Distributions of scaled jet pair mass for the four-jet events in their center-of-mass system. The statistical and total errors are represented by the inner and outer error bars, respectively. The data are also listed in Table VII.

The studies described above show that the QCD calculations agree well with the data. It is therefore interesting to examine the topological distributions of these subprocesses. Figures 13(a) and 13(b) show the x_4 and $\cos\theta_4^*$ distributions of the three-jet events and Figs. 13(c) and 13(d) show the x_5 and $\cos\theta_5^*$ distributions of the four-jet events predicted by the exact tree-level QCD calculations (full QCD) and by the QCD calculations of the three subprocesses. The full QCD is normalized to unit area and the subprocesses are normalized to the fractional contribution to their respective total cross section. The data distributions are normalized to the respective QCD distributions. The distributions of the subprocesses are remarkably similar and agree well with the data. The six-quark subprocess contributes less than 1% of the total cross section of the four-jet events and therefore is not shown in Figs. 13(c) and 13(d). Nevertheless, the normalized distributions are very similar to those of the other three subprocesses. The similarity of the subprocesses is observed in all other variables of the three- and four-jet events investigated in this paper. This suggests that the distributions are insensitive to the relative contributions of these subprocesses to the total cross section and therefore have weak dependences on the quark-gluon content in parton distribution functions. Furthermore, Rutherford characteristics are visible in $\cos\theta^*$ distributions for all subprocesses, implying that the matrix ele-

TABLE VII. The measured distribution of scaled jet pair masses for the four-jet events in their center-of-mass system. The errors include both statistical and systematic errors.

μ_{ij}	$1/NdN/d\mu_{34}$	$1/NdN/d\mu_{35}$	$1/NdN/d\mu_{36}$	$1/NdN/d\mu_{45}$	$1/NdN/d\mu_{46}$	$1/NdN/d\mu_{56}$
0.00–0.03						
0.03–0.06						
0.06–0.09			0.11±0.03	0.25±0.04	0.33±0.05	0.57±0.07
0.09–0.12			0.46±0.07	0.78±0.09	1.00±0.11	1.77±0.16
0.12–0.15			1.12±0.16	1.51±0.17	1.96±0.20	3.31±0.28
0.15–0.18		0.04±0.02	1.59±0.17	2.12±0.18	2.79±0.19	4.54±0.23
0.18–0.21		0.10±0.03	2.06±0.18	2.55±0.18	3.45±0.17	5.24±0.25
0.21–0.24		0.19±0.05	3.01±0.21	2.77±0.20	4.26±0.20	4.77±0.27
0.24–0.27		0.34±0.07	3.39±0.21	2.99±0.20	4.32±0.20	3.98±0.23
0.27–0.30		0.62±0.10	3.60±0.19	3.49±0.21	4.01±0.19	3.16±0.19
0.30–0.33		1.24±0.14	3.90±0.21	3.33±0.18	3.59±0.22	2.31±0.19
0.33–0.36	0.06±0.02	1.57±0.13	3.48±0.22	2.92±0.21	2.87±0.22	1.64±0.14
0.36–0.39	0.09±0.03	2.13±0.15	3.10±0.20	2.97±0.21	2.13±0.24	1.04±0.13
0.39–0.42	0.11±0.03	2.89±0.16	2.81±0.21	2.71±0.26	1.40±0.21	0.59±0.10
0.42–0.45	0.24±0.05	3.52±0.20	2.04±0.21	2.25±0.22	0.83±0.13	0.28±0.05
0.45–0.48	0.60±0.10	4.37±0.24	1.58±0.22	1.47±0.20	0.37±0.06	0.09±0.02
0.48–0.51	1.05±0.12	4.91±0.24	0.80±0.11	0.94±0.13	0.02±0.01	
0.51–0.54	1.63±0.16	4.59±0.26	0.24±0.04	0.26±0.04		
0.54–0.57	2.73±0.19	3.63±0.32	0.04±0.01			
0.57–0.60	3.85±0.24	2.03±0.26				
0.60–0.63	3.79±0.19	0.89±0.12				
0.63–0.66	4.15±0.21	0.23±0.04				
0.66–0.69	3.67±0.19					
0.69–0.72	3.17±0.19					
0.72–0.75	2.64±0.19					
0.75–0.78	2.06±0.20					
0.78–0.81	1.58±0.17					
0.81–0.84	1.04±0.12					
0.84–0.87	0.55±0.09					
0.87–0.90	0.29±0.05					

ments of these subprocesses are dominated by the t-channel exchange.

COMPARISON WITH PARTON-SHOWER EVENT GENERATORS

As discussed above, the measured topological distributions of three- and four-jet events are reproduced well by the exact tree-level QCD calculations. However, in many investigations, parton-shower Monte Carlo event generators are used to model multijet production. Therefore, it is interesting to compare the data distributions with those predicted by parton-shower event generators.

As an example, the x_3 and $\cos\theta_3^*$ distributions of three-jet events and μ_{34} and μ_{56} distributions of four-jet events are shown in Fig. 14 for the data and for the HERWIG 5.8, ISAJET

TABLE VIII. The measured $\chi_{\rm BZ}$ and $\cos\theta_{\rm NR}$ distributions for the four-jet events. The errors include both statistical and systematic errors.

$\chi_{\rm BZ}$	$1/NdN/d\chi_{\rm BZ}$	$\cos\theta_{\rm NR}$	$1/NdN/d\cos\theta_{\rm NR}$
0.0–10.0	0.0073±0.0004	0.0–0.1	1.02±0.06
10.0–20.0	0.0079±0.0004	0.1–0.2	1.07±0.06
20.0–30.0	0.0089±0.0004	0.2–0.3	0.93±0.05
30.0–40.0	0.0103±0.0004	0.3–0.4	0.98±0.06
40.0–50.0	0.0108±0.0005	0.4–0.5	0.99±0.06
50.0–60.0	0.0123±0.0006	0.5–0.6	0.98±0.06
60.0–70.0	0.0132±0.0006	0.6–0.7	0.96±0.06
70.0–80.0	0.0146±0.0007	0.7–0.8	0.99±0.06
80.0–90.0	0.0148±0.0010	0.8–0.9	1.01±0.07

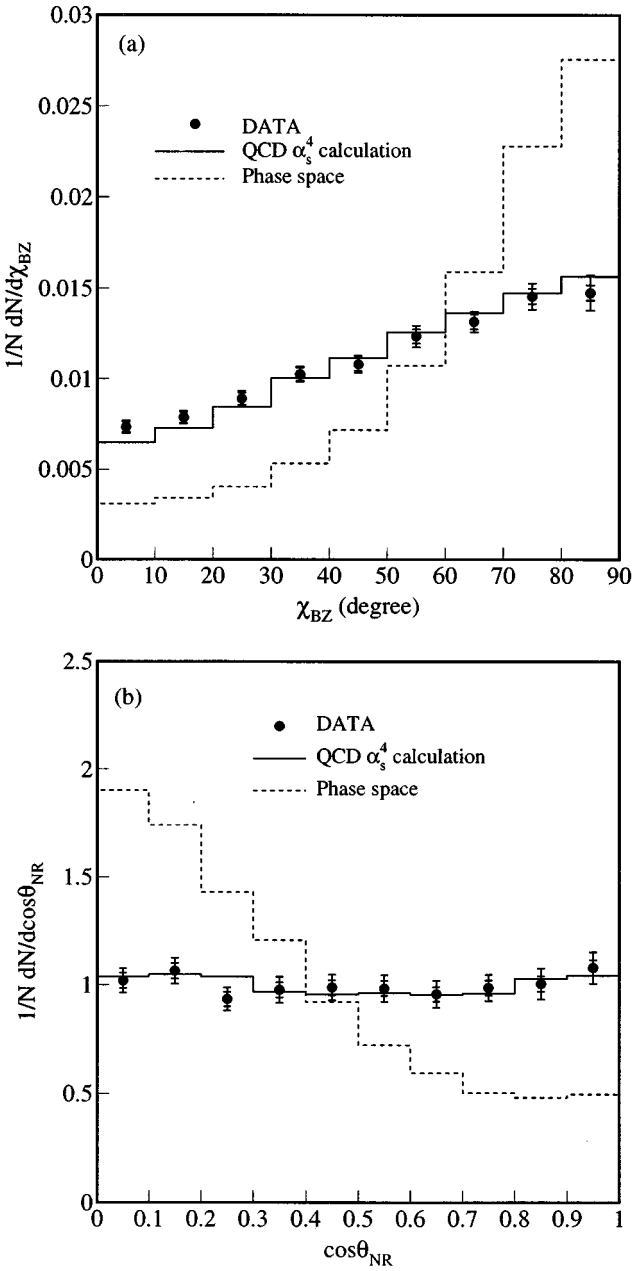

FIG. 12. The distribution of the angle between the planes of (a) the two leading jets and the two nonleading jets and (b) the momentum vector differences of the two leading jets and the two nonleading jets, for four-jet events in their center-of-mass system. The statistical and total errors are represented by the inner and outer error bars, respectively. The data are also listed in Table VIII.

7.13, and PYTHIA 5.6 parton-shower event generators.[2] The Monte Carlo distributions are calculated using parton jets which are formed by quarks and gluons after parton showering and before hadronization. The parton jets are initially reconstructed using a cone jet algorithm implemented in the PYTHIA program [21]. Then the jet direction is redefined using a D0 jet direction definition discussed above. Although the parton-shower generators describe the general structures of these variables well, differences in details are clearly visible. The largest difference is seen in the $\cos\theta_3^*$ distribution. All three parton-shower event generators show excessive contributions in the forward region.

To generate three- and four-jet events using the parton-shower generators, one has to start with $2\rightarrow2$ processes with a p_T cut and select events with hard gluon radiation. We note that a large fraction of the Monte Carlo events in the forward region which pass the 60 GeV leading jet E_T requirement have a $2\rightarrow2$ process with $p_T<50$ GeV/c. Presumably the leading jets of the these events are from hard initial-state radiation. This observation suggests that the initial-state radiation is not well modeled by these parton-shower generators in the phase-space region studied in this paper.

Although only four topological distributions are shown here, we have compared all other variables investigated in this paper. Apart from the $\cos\theta^*$ distributions, the HERWIG event generator provides a reasonably good description of the data while the differences between the data and the predictions of ISAJET and PYTHIA event generators are large in many distributions. Overall, the HERWIG event generator describes the data better than the ISAJET and the PYTHIA do.

SUMMARY

From the data sample recorded by the D0 detector in $\overline{pp}$ collisions at $\sqrt{s}=1800$ GeV at the Tevatron during the 1992–1993 running period, high-statistics three-jet and four-jet event samples have been selected. A large number of distributions characterizing the global structures of the inclusive three- and four-jet events have been compared with QCD calculations of the exact tree-level matrix elements and with calculations of QCD subprocesses involving different numbers of quarks. This paper extends earlier studies to previously untested regions of phase space for a large number of topological variables. All comparisons have been made with the parton-level distributions and based on normalized distributions rather than cross sections.

For the three-jet events, the investigated topological variables are the energy fractions carried by the two leading jets, the cosine of the leading jet polar angle, the angle between the plane containing the leading jet and the beam line, the plane containing the two nonleading jets, and the scaled invariant masses of the jet pairs. In the case of the four-jet events, the energy fractions and the cosines of the polar angles of all four jets, the six opening angles, scaled invariant masses of jet pairs, and the angles between jet planes have been studied.

Studies show that the measured topological distributions of the three- and four-jet events are well reproduced by the exact tree-level matrix elements QCD calculations. The good agreement implies that the topological distributions of the three- and four-jet events are consistent with the tree-level diagrams and therefore the topological distributions are not very sensitive to higher-order corrections. Furthermore, the distributions are found to be insensitive to the uncertainties in parton distribution functions and to the quark-gluon flavor of the underlying partons. The dominance of the t-channel gluon exchange to a large extent determines the structure of the event. The differences between the data and the phase-

[2]All parton-shower events are generated with a $p_T=10$ GeV/c cutoff for the initial $2\rightarrow2$ hard scattering, using their default parameters.

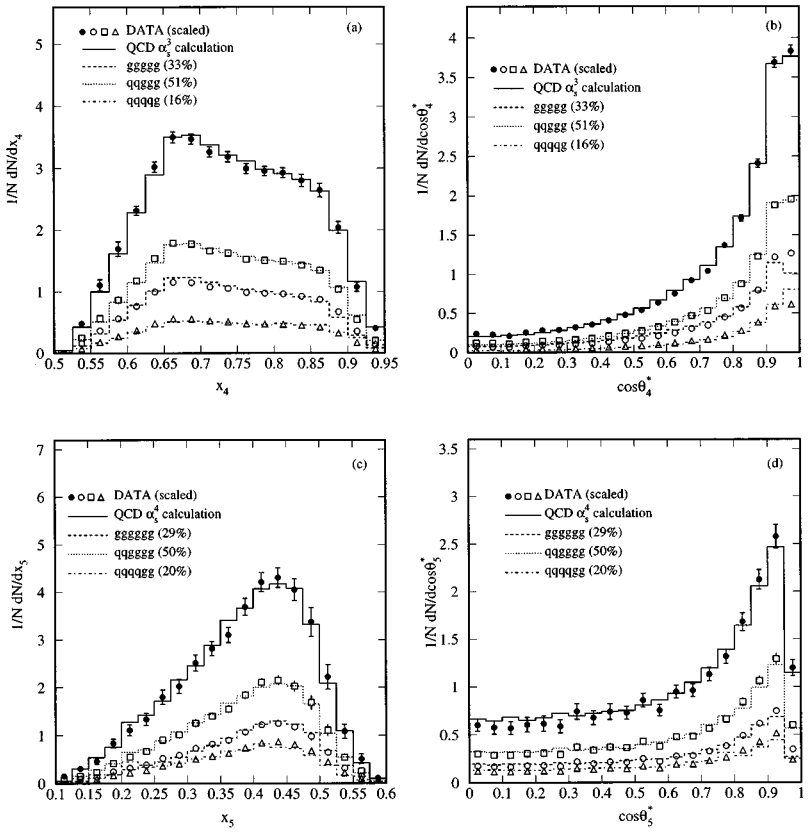

FIG. 13. The (a) x_4 and (b) $\cos\theta_4^*$ distributions for three-jet events and the (c) x_5 and (d) $\cos\theta_5^*$ distributions for four-jet events in their center-of-mass system. The QCD subprocesses are normalized to their fractional contributions to the respective total cross section for the selection criteria described in the text. The data are scaled to the normalization of the respective subprocess of the QCD calculation. Therefore, only the shapes of the subprocesses are compared. The error bars on the data include both statistical and systematic errors.

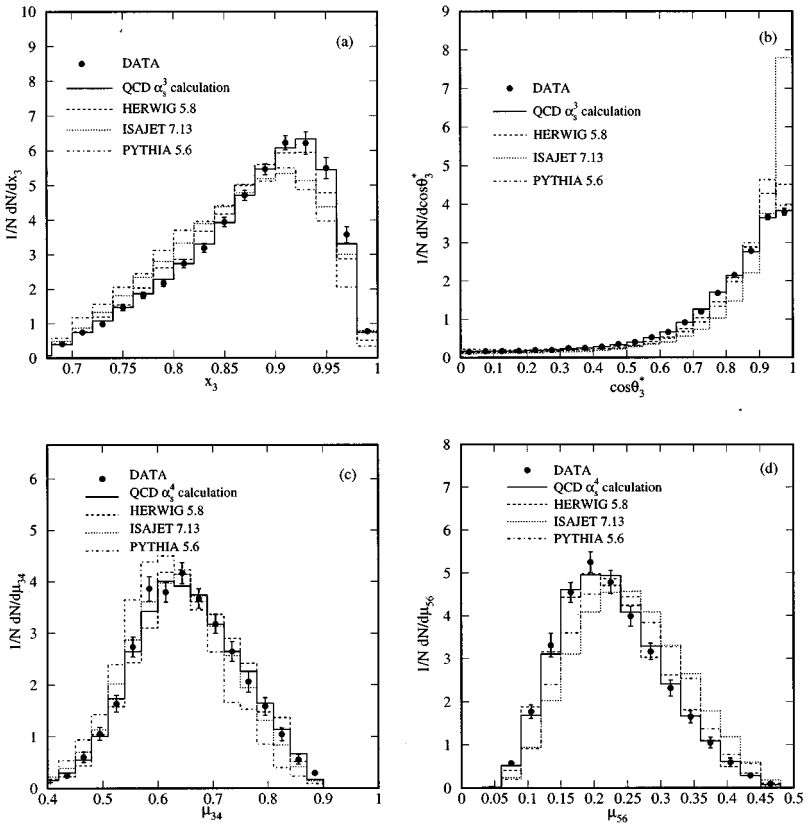

FIG. 14. Comparisons between the data, exact tree-level QCD calculations, and HERWIG, ISAJET, and PYTHIA Monte Carlo predictions. Shown are (a) the scaled energy of the leading jet and (b) the cosine of the leading jet for three-jet events, and the scaled invariant mass distributions of (c) the two leading jets and (d) the two nonleading jets for four-jet events. The error bars on the data include both statistical and systematic errors.

space model are large for most of the distributions. Finally, we note that apart from the $\cos\theta^*$ distributions, the HERWIG 5.8 event generator provides a good description of the measured distributions while the differences between the data and the predictions of the ISAJET 7.13 and the PYTHIA 5.6 event generators are relatively large in many distributions.

ACKNOWLEDGMENTS

We thank the Fermilab Accelerator, Computing, and Research Divisions, and the support staffs at the collaborating institutions for their contributions to the success of this work. We also acknowledge the support of the U.S. Department of Energy, the U.S. National Science Foundation, the Commissariat à L'Energie Atomique in France, the Ministry for Atomic Energy and the Ministry of Science and Technology Policy in Russia, CNPq in Brazil, the Departments of Atomic Energy and Science and Education in India, Colciencias in Colombia, CONACyT in Mexico, the Ministry of Education, Research Foundation and KOSEF in Korea, and the A.P. Sloan Foundation.

[1] M. Gell-Mann, Acta Phys. Austriaca, Suppl. **9**, 733 (1972); H. Fritzsch and M. Gell-Mann, in proceedings of the 16th International Conference on High Energy Physics, Batavia, 1972, edited by J.D. Jackson and A. Roberts, National Accelerator Laboratory, 1972 (unpublished); H. Fritzsch, M. Gell-Mann, and H. Leutwyler, Phys. Lett. **47B**, 365 (1973).

[2] D.J. Gross and F. Wilczek, Phys. Rev. Lett. **30**, 1343 (1973); Phys. Rev. D **8**, 3633 (1973); H.D. Politzer, Phys. Rev. Lett. **30**, 1346 (1973).

[3] G. 't Hooft, Nucl. Phys. **B33**, 173 (1971).

[4] For recent reviews on QCD tests at e^+e^- collider see S. Bethke and J.E. Pilcher, Annu. Rev. Nucl. Part. Sci. **42**, 251 (1992); T. Hebbeker, Phys. Rep. **217**, 69 (1992).

[5] For recent reviews on QCD tests at $\overline{p}p$ collider see J.E. Huth and M.L. Mangano, Annu. Rev. Nucl. Part. Phys. **43**, 585 (1993); R.K. Ellis and W.J. Stirling, Fermilab Report No. Fermilab-Conf-90/164-T, 1990 (unpublished).

[6] V.D. Elvira, in Proceedings of the 8th Meeting of the APS Division of Particles and Fields, Albuquerque, 1994 (unpublished).

[7] UA1 Collaboration, G. Arnison *et al.*, Phys. Lett. **158B**, 494 (1985); UA2 Collaboration, J.A. Appel *et al.*, Z. Phys. C **30**, 341 (1986).

[8] CDF Collaboration, F. Abe *et al.*, Phys. Rev. D **45**, 1448 (1992).

[9] UA2 Collaboration, J. Alitti *et al.*, Phys. Lett. B **268**, 145 (1991).

[10] CDF Collaboration, F. Abe *et al.*, Phys. Rev. D **45**, 2249 (1992); Phys. Rev. Lett. **75**, 608 (1995).

[11] M. Bengtsson and P.M. Zerwas, Phys. Lett. B **208**, 306 (1988).

[12] O. Nachtmann and A. Reiter, Z. Phys. C **16**, 45 (1982).

[13] Z. Kunszt and E. Pietarinen, Nucl. Phys. **B164**, 45 (1980); T. Gottschalk and D. Sivers, Phys. Rev. D **21**, 102 (1980); F.A. Berends *et al.*, Phys. Lett. B **118**, 124 (1981).

[14] F.A. Berends, W.T. Giele, and H. Kuijf, Nucl. Phys. **B333**, 120 (1990); Phys. Lett. B **232**, 266 (1990).

[15] Z. Kunszt and W.J. Stirling, Phys. Lett. B **171**, 307 (1986); Phys. Rev. D **56**, 2439 (1988).

[16] C.J. Maxwell, Phys. Lett. B **192**, 190 (1987); Nucl. Phys. **B316**, 321 (1989); M.L. Mangano and S.J. Parke, Phys. Rev. D **39**, 758 (1989); C.J. Maxwell and S.J. Parke, *ibid.* **44**, 2727 (1991).

[17] I. Hinchliffe, LBL Report No. LBL-34372, 1993 (unpublished).

[18] K. Konishi, A. Ukawa, and G. Veneziano, Nucl. Phys. **B157**, 45 (1979); R. Odorico, *ibid.* **B172**, 157 (1980); G.C. Fox and S. Wolfram, *ibid.* **B168**, 285 (1980); T.D. Gottschalk, *ibid.* **B214**, 201 (1983); G. Marchesini and B.R. Webber, *ibid.* **B238**, 1 (1984); B.R. Webber, *ibid.* **B238**, 492 (1984).

[19] Computer code HERWIG 5.8, G. Marchesini and B. Webber, Nucl. Phys. **B310**, 461 (1988); I.G. Knowles, *ibid.* **B310**, 571 (1988); G. Marchesini *et al.*, Comput. Phys. Commun. **67**, 465 (1992).

[20] Computer code ISAJET 7.13, F. Paige and S. Protopopescu, BNL Report No. BNL38034, 1986 (unpublished).

[21] Computer code PYTHIA 5.6, H.U. Bengtsson and T. Sjöstrand, Comput. Phys. Commun. **46**, 43 (1987).

[22] V.D. Elvira, Ph.D thesis, Universidad de Buenos Aires, Argentina, 1995.

[23] D0 Collaboration, S. Abachi *et al.*, Nucl. Instrum. Methods Phys. Res. A **338**, 185 (1994).

[24] J. Linnemann, in Proceedings of the 7th Meeting of the APS Division of Particles and Fields, Batavia, 1992 (unpublished).

[25] Particle Data Group, K. Hikasa *et al.*, Phys. Rev. D **45**, II.1 (1992).

[26] J. Kotcher, in Proceedings of the 1994 Beijing Calorimetry Symposium, edited by H.S. Chen, Beijing, China, 1994 (unpublished), p. 144. H. Weerts, in Proceedings of 9th Topical Workshop on Proton-Antiproton Collider Physics, edited by K. Kondo and S. Kim (Universal Academy Press, Tokyo, 1994), p. 192.

[27] A.D. Martin, R.G. Roberts, and W.J. Stirling, Phys. Rev. D **37**, 1161 (1988); Phys. Lett. B **206**, 327 (1988); Mod. Phys. Lett. A **4**, 1135 (1989).

[28] E. Eichten, I. Hinchliffe, K. Lane, and C. Quigg, Rev. Mod. Phys. **56**, 579 (1984); Rev. Mod. Phys. **58**, 1065 (1985).

[29] J. Morfin and W.K. Tung, Z. Phys. C **52**, 13 (1991).

[30] W.T. Giele (private communication).

[31] A.J. Milder, Ph.D. thesis, University of Arizona, Tucson, 1993.